

# Intramolecular Hydrogen Shift Chemistry of Hydroperoxy-Substituted Peroxy Radicals

Eric Praske,<sup>†</sup> Rasmus V. Otkjær,<sup>‡</sup> John D. Crouse,<sup>§</sup> J. Caleb Hethcox,<sup>†</sup> Brian M. Stoltz,<sup>†</sup> Henrik G. Kjaergaard,<sup>\*,‡</sup> and Paul O. Wennberg<sup>\*,§,⊥</sup>

<sup>†</sup>Division of Chemistry and Chemical Engineering, California Institute of Technology, 1200 East California Boulevard, Pasadena, California 91125, United States

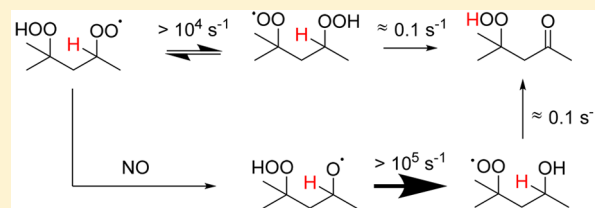
<sup>‡</sup>Department of Chemistry, University of Copenhagen, Universitetsparken 5, DK-2100 Copenhagen Ø, Denmark

<sup>§</sup>Division of Geological and Planetary Sciences, California Institute of Technology, 1200 East California Boulevard, Pasadena, California 91125, United States

<sup>⊥</sup>Division of Engineering and Applied Science, California Institute of Technology, 1200 East California Boulevard, Pasadena, California 91125, United States

## Supporting Information

**ABSTRACT:** Gas-phase autoxidation – the sequential regeneration of peroxy radicals (RO<sub>2</sub>) via intramolecular hydrogen shifts (H-shifts) followed by oxygen addition – leads to the formation of organic hydroperoxides. The atmospheric fate of these peroxides remains unclear, including the potential for further H-shift chemistry. Here, we report H-shift rate coefficients for a system of RO<sub>2</sub> with hydroperoxide functionality produced in the OH-initiated oxidation of 2-hydroperoxy-2-methylpentane. The initial RO<sub>2</sub> formed in this chemistry are unable to undergo α-OOH H-shift (HOOC–H) reactions. However, these RO<sub>2</sub> rapidly isomerize (>100 s<sup>-1</sup> at 296 K) by H-shift of the hydroperoxy hydrogen (ROO–H) to produce a hydroperoxy-substituted RO<sub>2</sub> with an accessible α-OOH hydrogen. First order rate coefficients for the 1,5 H-shift of the α-OOH hydrogen are measured to be ~0.04 s<sup>-1</sup> (296 K) and ~0.1 s<sup>-1</sup> (318 K), within 50% of the rate coefficients calculated using multifragment transition state theory. Reaction of the RO<sub>2</sub> with NO produces alkoxy radicals which also undergo rapid isomerization via 1,6 and 1,5 H-shift of the hydroperoxy hydrogen (ROO–H) to produce RO<sub>2</sub> with alcohol functionality. One of these hydroxy-substituted RO<sub>2</sub> exhibits a 1,5 α-OH (HOC–H) H-shift, measured to be ~0.2 s<sup>-1</sup> (296 K) and ~0.6 s<sup>-1</sup> (318 K), again in agreement with the calculated rates. Thus, the rapid shift of hydroperoxy hydrogens in alkoxy and peroxy radicals enables intramolecular reactions that would otherwise be inaccessible.



## INTRODUCTION

In the atmosphere, organic peroxy radicals (RO<sub>2</sub>) are formed following the reaction of OH, NO<sub>3</sub>, or O<sub>3</sub> with hydrocarbons.<sup>1</sup> These RO<sub>2</sub> radicals undergo bimolecular reaction with NO, HO<sub>2</sub>, and other RO<sub>2</sub> radicals.<sup>2</sup> In addition, unimolecular reactions of RO<sub>2</sub> have recently been shown to be important in the atmospheric chemistry of a growing number of hydrocarbons.<sup>3–14</sup> These reactions form the basis of gas-phase autoxidation, which involves the regenerative formation of RO<sub>2</sub> via intramolecular RO<sub>2</sub> H-shifts followed by O<sub>2</sub> addition. These reactions proceed through hydroperoxy alkyl radical intermediates, often denoted QOOH.<sup>15</sup> Such chemistry has long been known to be relevant in combustion.<sup>16,17</sup>

Atmospheric autoxidation has been implicated in the rapid oxygenation of hydrocarbons, contributing to new particle formation and growth.<sup>18–31</sup> Autoxidation was recently shown to play a role in the oxidation of alkanes emitted in urban areas.<sup>32</sup> Hydroxy-substituted RO<sub>2</sub> radicals are produced in this chemistry and exhibit sufficiently low energetic barriers for H-shift reactions that compete with bimolecular reactions in the

atmosphere.<sup>33</sup> Indeed, some of these H-shift rates are sufficiently fast (~0.1 s<sup>-1</sup>) that multifunctional organic hydroperoxides can be produced via this mechanism even under modestly polluted conditions. The fate of these hydroperoxides in urban air, however, remains largely unexplored. It is possible that these hydroperoxides partition to the aerosol phase or photolyze due to enhanced absorption cross sections.<sup>34,35</sup> In the gas phase, organic hydroperoxides will undergo further reaction with OH to produce hydroperoxy-substituted RO<sub>2</sub>. Intramolecular H-shifts in these radicals have been the subject of previous studies, but only at elevated temperature.<sup>36–43</sup>

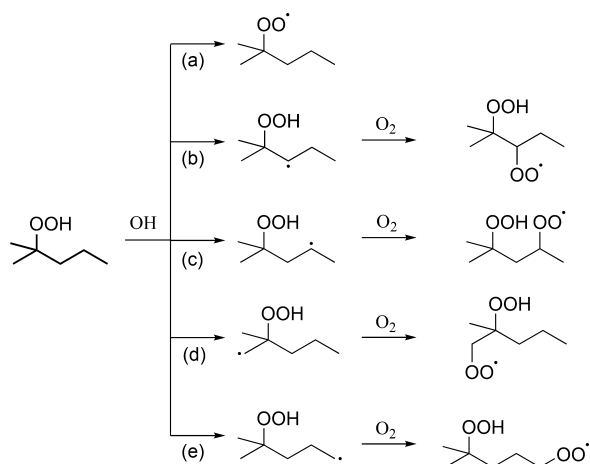
In this study, we oxidize 2-hydroperoxy-2-methylpentane with OH under conditions relevant to the atmosphere. As shown in Scheme 1, the RO<sub>2</sub> formed following hydrogen abstraction and O<sub>2</sub> addition lack an abstractable α-OOH

Received: October 5, 2018

Revised: December 10, 2018

Published: December 14, 2018

**Scheme 1. Peroxy Radicals (RO<sub>2</sub>) Formed Following OH-Initiated Oxidation of 2-Hydroperoxy-2-methylpentane<sup>a</sup>**

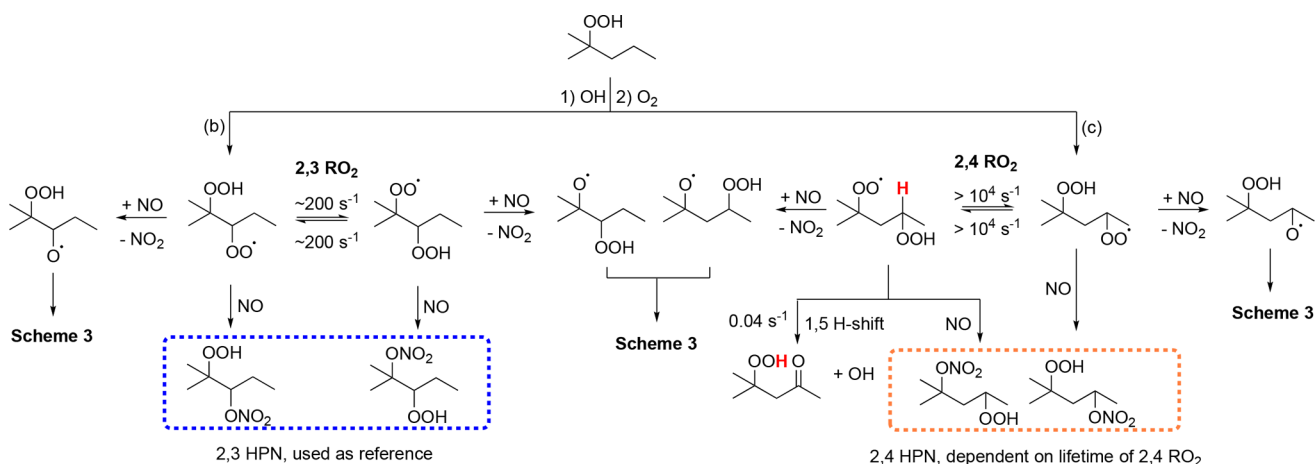


<sup>a</sup>Abstraction of the hydroperoxide hydrogen is a major channel (a). Abstraction of secondary alkyl hydrogens (b, c) dominates over that of primary alkyl hydrogens (d, e).

hydrogen due to the presence of the methyl substituent. However, due to rapid and reversible H-shifts between the ROO–H and the RO<sub>2</sub> radical centers, an RO<sub>2</sub> with an accessible  $\alpha$ -OOH hydrogen is produced. The dominant channels (b and c) are illustrated in Scheme 2. In the presence of NO, these RO<sub>2</sub> form distinct hydroperoxynitrates (HPN) that are quantified in this work (shown in boxes).

In addition to HPN, reaction of the RO<sub>2</sub> with NO produces alkoxy radicals (Scheme 3). These alkoxy radicals undergo a very rapid H-shift with hydroperoxy hydrogens to produce hydroxy-substituted RO<sub>2</sub>. One of these hydroxy-substituted RO<sub>2</sub> possesses an accessible 1,5  $\alpha$ -OH H-shift. Due to the ability to unlock alkyl H-shifts that would otherwise be inaccessible (or very slow), the rapid isomerization of hydroperoxy-substituted alkoxy and peroxy radicals represents a critical process in the oxidation mechanism of the substrate

**Scheme 2. RO<sub>2</sub> Formed Following Pathways b and c in Scheme 1 That Undergo Rapid H-Shifts of the Hydroperoxy Hydrogen, Producing Two Pairs of RO<sub>2</sub> (Denoted Here as 2,3 and 2,4 RO<sub>2</sub>)<sup>a</sup>**



<sup>a</sup>In the presence of NO, these RO<sub>2</sub> form distinct hydroperoxynitrates (HPN) that are quantified in this work (shown in boxes). For the 4-hydroperoxy-2-methyl-2-peroxy isomer of the 2,4 RO<sub>2</sub>, a unimolecular 1,5  $\alpha$ -OOH H-shift competes with the bimolecular reaction with NO. The forward rate coefficients shown are those measured at 296 K. The reverse rate coefficients for the 2,3 and 2,4 RO<sub>2</sub> are similar given the measured distribution of the products of the two sets of isomers.

used here as well as many other compounds found in the urban atmosphere. This rapid isomerization between ROOH and RO<sub>2</sub>, first described in a computational study by Jørgensen and co-workers,<sup>44,45</sup> is similar to the interconversion of alcohols and alkoxy radicals reported in computational studies by Dibble.<sup>46,47</sup>

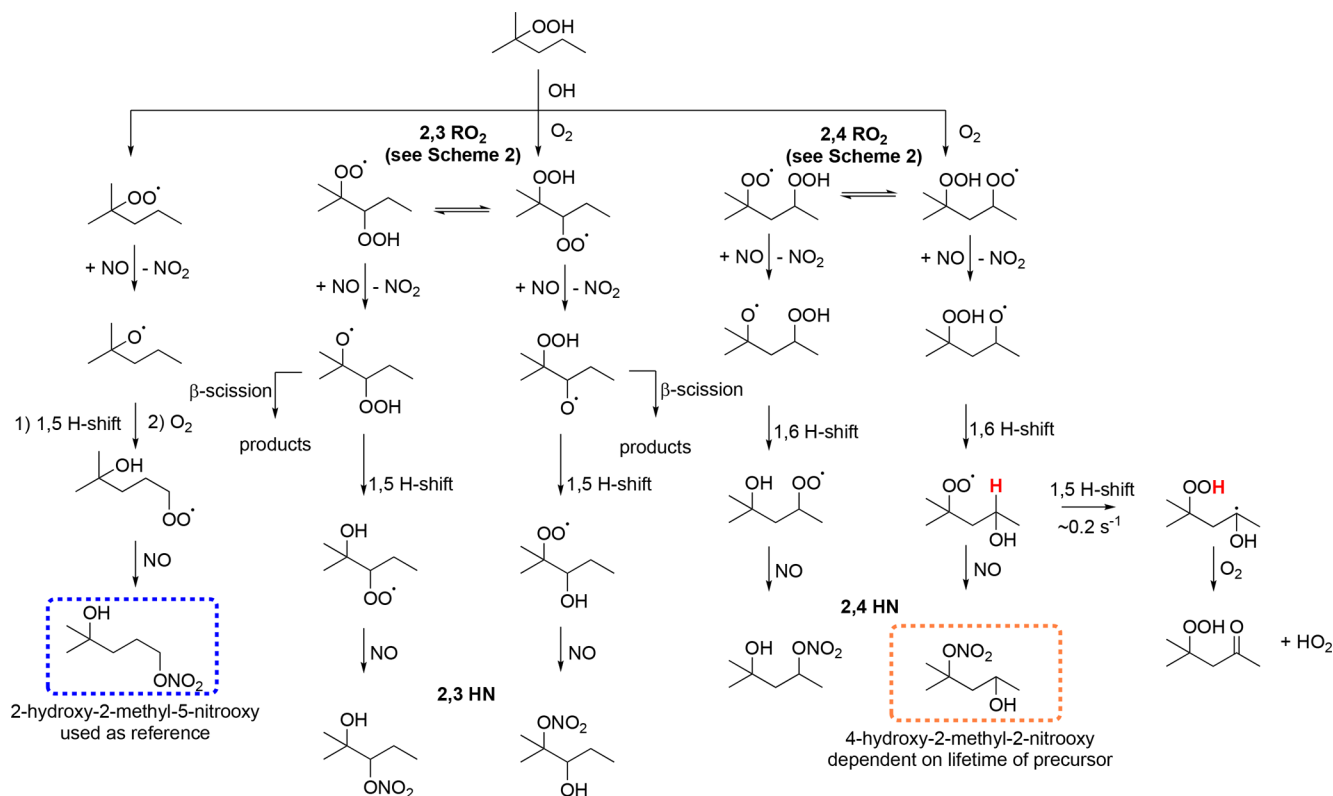
## METHODS

**Theory.** Multiconformer transition state theory (MC-TST) is used to calculate the rate coefficients in this work.<sup>48–51</sup> MC-TST is well-suited to characterize intramolecular RO<sub>2</sub> chemistry due to the large number of reactant conformers typically encountered. We follow the MC-TST approach of Møller et al.,<sup>51</sup> which has been shown to provide good agreement with the few available measured H-shift rate coefficients.<sup>32</sup> The MC-TST expression for the rate coefficient is

$$k_{MC-TST} = \kappa \frac{k_B T}{h} \frac{\sum_i^{\text{all TS conf.}} \exp\left(-\frac{\Delta E_i}{k_B T}\right) Q_{TS,i}}{\sum_j^{\text{all R conf.}} \exp\left(-\frac{\Delta E_j}{k_B T}\right) Q_{R,j}} \times \exp\left(-\frac{E_{TS,0} - E_{R,0}}{k_B T}\right)$$

where  $h$  is Planck's constant,  $k_B$  is Boltzmann's constant, and  $T$  is the temperature.  $\Delta E_i$  is the zero-point corrected energy difference between TS conformer  $i$  and the lowest energy TS conformer,  $Q_{TS,i}$  is the partition function of TS conformer  $i$ , and  $E_{TS,0}$  is the zero-point corrected energy of the lowest energy TS conformer. The symbols are analogously defined for the reactant conformers.  $\kappa$  is the Eckart tunneling correction factor (see Supporting Information for further details).<sup>52</sup>

Conformers are located with a systematic Merck Molecular Force Field (MMFF)<sup>53–58</sup> conformer search in Spartan'14,<sup>59</sup> with the radical atom forced to have no charge.<sup>51</sup> Conformers are then optimized with B3LYP/6-31+G(d) in Gaussian 09.<sup>60–65</sup> We calculate the vibrational frequencies of the

Scheme 3. Pathways Following Reaction of RO<sub>2</sub> with NO<sup>a</sup>

<sup>a</sup>In addition to the organonitrate pathway shown in Scheme 2, the reaction of RO<sub>2</sub> with NO produces alkoxy radicals. These alkoxy radicals rapidly isomerize to produce hydroxy RO<sub>2</sub> which react with NO to produce hydroxy nitrates (HN - boxes) and other products. The 4-hydroxy-2-methyl-2-peroxy RO<sub>2</sub> can also undergo a 1,5  $\alpha$ -OH H-shift.  $\beta$ -Scission is only expected to be competitive for the 2,3 alkoxy radicals, and thus this pathway is omitted in the scheme for the remaining alkoxy radicals.

conformers to verify that a minimum or first-order saddle point was found as desired. Duplicate conformers are removed by a custom bash-wrapped python script, by comparing dipole moments and energies.<sup>66</sup> Zero-point energy corrected conformers within 2 kcal/mol of the lowest energy conformer are reoptimized with  $\omega$ B97X-D/aug-cc-pVTZ ( $\omega$ B97) and their frequencies are calculated.<sup>67,68</sup> The energies and partition functions at this level are used for the  $\Delta E$ s and  $Q$ s in the MC-TST expression. For the lowest energy conformer of reactant and TS, we calculate a ROHF-ROCCSD(T)-F12a/VDZ-F12// $\omega$ B97X-D/aug-cc-pVTZ<sup>69-73</sup> (F12) single-point energy with MOLPRO 2012<sup>74</sup> to use with the  $\omega$ B97 zero-point correction for accurate values of  $E_{TS,0}$  and  $E_{R,0}$ . For the rapid alkoxy (RO) and peroxy (RO<sub>2</sub>) ROO-H H-shift reactions, the reaction barriers were calculated at the  $\omega$ B97 level due to convergence problems with the F12 energies in the TS of these reactions. This causes an increase in the uncertainty of the barrier (and, to a minor extent, tunneling) of these calculated H-shifts and the rate coefficients are accurate to about a factor of 100. The ratios of the equilibrated RO<sub>2</sub> isomers are independent of the TS and are obtained at the F12 level.

**Experiment.** Using a method analogous to that of our earlier study of hexane oxidation,<sup>32</sup> we use isomer-specific measurements of multifunctional organonitrates (RONO<sub>2</sub>) to study the rate coefficients of unimolecular chemistry. RO<sub>2</sub> undergoing unimolecular chemistry will have smaller yields of HPN at longer bimolecular lifetimes. For the hydroperoxy-substituted RO<sub>2</sub>, the equilibrated isomer will also have smaller yields of HPN. By quantifying the yields of the HPN as a

function of the bimolecular lifetime, we determine the rate coefficients of the H-shift chemistry.

**Materials and Hydroperoxide Synthesis.** 2-Methyl-2-pentene (98%, Fluka), 2-propanol ( $\geq 99\%$ , Macron), and nitric oxide ( $1993 \pm 20$  ppmv NO in N<sub>2</sub>, Matheson) are used as purchased. CH<sub>3</sub>ONO is synthesized in a manner similar to that described by Taylor et al.<sup>75</sup>

2-hydroperoxy-2-methylpentane is synthesized by addition of 2-methyl-2-pentanol (2.5 g, 24.5 mmol) as a solution in ether (8 mL) to a mixture of 30% aqueous hydrogen peroxide (30 mL) and 10 M H<sub>2</sub>SO<sub>4</sub> (3 mL), and the mixture is stirred for 18 h. The reaction is quenched with saturated K<sub>2</sub>CO<sub>3</sub> (10 mL), and the layers are separated. The organic layer is washed with brine (8 mL), dried (Na<sub>2</sub>SO<sub>4</sub>), and concentrated under reduced pressure. The crude reaction mixture, purified via flash column chromatography, elutes with CH<sub>2</sub>Cl<sub>2</sub>/Et<sub>2</sub>O (25:1) on SiO<sub>2</sub> (50 mL) to provide 2.14 g (74%) of 2-hydroperoxy-2-methylpentane as a colorless liquid. Refer to the [Supporting Information](#) for the characterization of this compound.

**Chamber Studies.** 2-Hydroperoxy-2-methylpentane is added to a  $\sim 1$  m<sup>3</sup> Teflon chamber via evaporation of an aqueous solution prepared by mixing the neat peroxide with water (1:1 by volume). A small quantity ( $< 4$   $\mu$ L) of this solution is placed in a 3-way vial and zero air transfers the headspace to the chamber. CH<sub>3</sub>ONO is introduced to the chamber via a 500 mL glass bulb. FTIR (Nicolet 560 Magna IR) is used to quantify the contents of the bulb prior to addition using published absorption cross sections.<sup>76</sup> Nitric

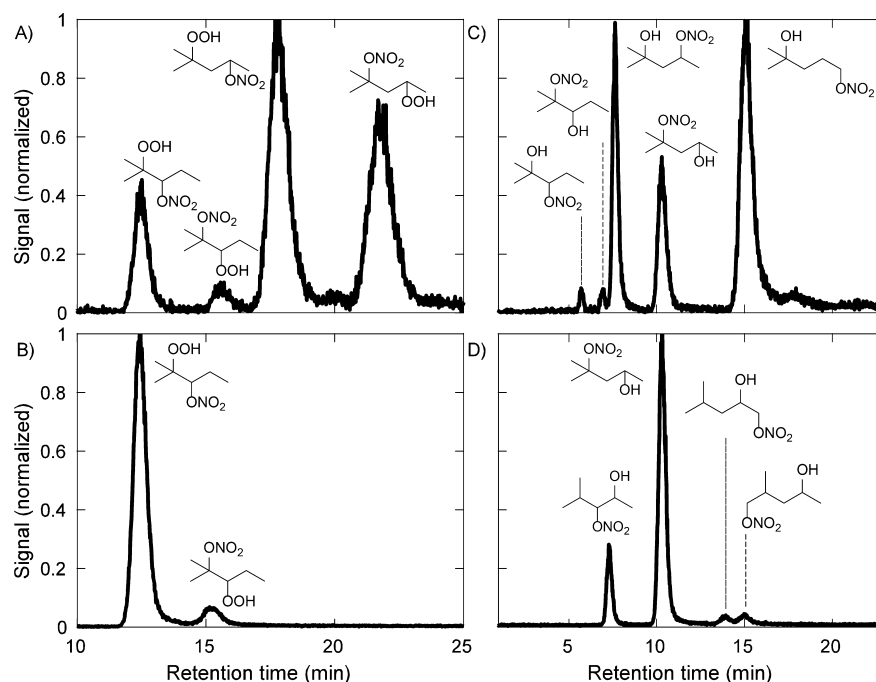
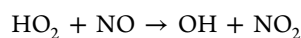


**Figure 1.** RONO<sub>2</sub> are separated and identified by GC–CIMS. Chromatographic assignment of the HPN (clustered with CF<sub>3</sub>O<sup>−</sup> at *m/z* 264): (A) OH-initiated oxidation of 2-hydroperoxy-2-methylpentane; (B) NO<sub>3</sub>-initiated oxidation of 2-methyl-2-pentene (see Scheme 4A) produced the 2,3 HPN isomers. Chromatographic assignment of the HN (*m/z* 248): (C) OH-initiated oxidation of 2-hydroperoxy-2-methylpentane. Note the relatively lower abundance of the 2,3 HN as compared to the 2,3 HPN in panel A. As discussed in the text, we attribute this to the fast decomposition of the 2,3 alkoxy radicals, which outruns the 1,5 alkoxy H-shift of the hydroperoxide hydrogen (see Scheme 3). (D) OH-initiated oxidation of 4-methyl-2-pentanol (see Scheme 4B) primarily produced the tertiary HN. In each of the chromatograms, the signal has been normalized to the intensity of the tallest peak.

oxide is introduced in some experiments and is quantified using a Teledyne 200 EU NO<sub>x</sub> analyzer.

Sylvania blacklights ( $\lambda_{\max} \sim 350$  nm) illuminate the chamber for between 10 min and 16 h following the collection of background chromatograms. Photolysis of CH<sub>3</sub>ONO in air produces NO, HO<sub>2</sub>, and OH:



$$\tau_{\text{bimolecular}} = \frac{1}{k_{\text{RO}_2+\text{NO}}[\text{NO}] + k_{\text{RO}_2+\text{HO}_2}[\text{HO}_2]}$$

$$= \frac{1}{k_{\text{bimolecular}}} \quad (1)$$

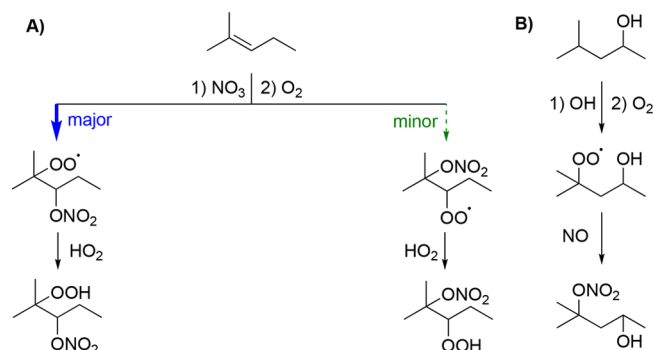
By using a low abundance of the organic peroxide ( $\sim 20$ – $80$  ppbv), the impact of RO<sub>2</sub> + RO<sub>2</sub> chemistry is minimized. Determination of  $\tau_{\text{bimolecular}}$  is described in the Supporting Information. The ratio  $\frac{k_{\text{RO}_2+\text{NO}}}{k_{\text{RO}_2+\text{HO}_2}}$  is assumed to be the same for RO<sub>2</sub> isomers.

Following oxidation of a small amount (5–20%) of the 2-hydroperoxy-2-methylpentane, the lights are turned off and isomer specific measurement of RONO<sub>2</sub> is performed using a gas chromatograph chemical ionization mass spectrometer (GC–CIMS),<sup>77</sup> following the method described previously in Prasko et al.<sup>32</sup> Briefly, the output of a GC equipped with an 11.5 m Restek RTX-200 column is coupled to the CIMS, using CF<sub>3</sub>O<sup>−</sup> (*m/z* 85) as the reagent ion.<sup>78–82</sup> Following cryofocusing of the analytes on the head of the column, a

temperature program is initiated. See the Supporting Information for further details.

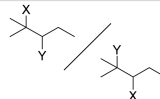
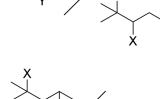
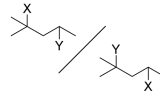
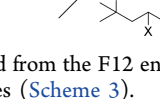
**Chromatographic Assignment of RONO<sub>2</sub>.** Four major HPN isomers are resolved following oxidation of 2-hydroperoxy-2-methylpentane by OH in the presence of NO (Figure 1A). As discussed below and shown in Scheme 2, these are produced from two pairs of interconverting hydroperoxy peroxy radicals with the functional groups either  $\beta$  (2,3) or  $\gamma$  (2,4). The two 2,3 HPN are assigned using the NO<sub>3</sub>-initiated oxidation of 2-methyl-2-pentene (see Scheme 4A). This chemistry produces nitrooxy peroxy radicals that react with

#### Scheme 4. Chromatographic Assignment Based on the Oxidation of Commercially Available Precursors<sup>a</sup>



<sup>a</sup>Key: (A) The NO<sub>3</sub>-initiated oxidation of 2-methyl-2-pentene produced the 2,3 HPN from 2-hydroperoxy-2-methylpentane. (B) The OH-initiated oxidation of 4-methyl-2-pentanol produces the HN isomer shown in the orange box in Scheme 3.

Table 1. Comparison of Calculated Ratio of the Equilibrated RO<sub>2</sub> Isomers and the Measured Ratio of Their Products<sup>a</sup>

Ratio	Temperature (K)	RO <sub>2</sub> <sup>a</sup> (X=OO; Y=OOH)	HPN <sup>b</sup> (X=ONO <sub>2</sub> ; Y=OOH)	HN <sup>c</sup> (X=OH; Y=ONO <sub>2</sub> )
	296	0.59	0.31 ± 0.02	-
	318	0.71	0.34 ± 0.04	-
	296	3.1	0.75 ± 0.06	1.3 ± 0.1
	318	3.3	0.77 ± 0.06	1.4 ± 0.1

<sup>a</sup>Key: (a) The ratio calculated from the F12 energies of the RO<sub>2</sub>. (b) The ratio of the measured hydroperoxy nitrates (Scheme 2). (c) The ratio of the measured hydroxy nitrates (Scheme 3).

HO<sub>2</sub> produced via reaction of NO<sub>3</sub> with HCHO, as described by Schwantes et al.<sup>83</sup> NO<sub>3</sub> preferentially adds to the secondary carbon of the olefin.<sup>83</sup> As shown in Figure 1B, we observe the formation of two HPN in a ratio of ~10:1 and thus assign the first peak (largest) to the secondary nitrate. The remaining two peaks in Figure 1A are assigned to the 2,4 HPN isomers. This is consistent with previous observations that the retention time of analytes with the same functionality generally increases with increasing separation of the functional groups.<sup>32,84</sup>

To assign the hydroxy-substituted nitrates (HN) produced in the oxidation of 2-hydroperoxy-2-methylpentane (Figure 1C), we use measurements of the products of the OH-initiated oxidation of 4-methyl-2-pentanol (see Scheme 4B and Figure 1D). The tertiary HN is the major HN produced from this chemistry and allows assignment of the HN eluting at this time as the 4-hydroxy-2-methyl-2-nitrooxy isomer. The remaining isomers are assigned based on elution order. We assume, as shown in the oxidation of 2-methyl-2-pentene, that secondary nitrates elute first. Thus, the preceding peak in Figure 1C is inferred to correspond to the 2-hydroxy-2-methyl-4-nitrooxy isomer while the later eluting isomer is assigned to the 2-hydroxy-2-methyl-5-nitrooxy isomer. Finally, we assume that the first two smaller peaks correspond to the 2,3 HN. As discussed below, we interpret their much smaller abundance (compared with that of the 2,3 HPN) as reflecting competition between  $\beta$ -scission and the ROO-H shift to the alkoxy radical (Scheme 3). Further evidence for the assignments in both the hydroperoxides (and alcohols) is shown in the Supporting Information (Figure S7) where, at very high NO concentrations, we are able to capture the distribution of 2,3 HPN and HN before the 2,3 RO<sub>2</sub> are fully equilibrated, and thereby assign the tertiary hydroperoxide (and secondary alcohol).

## RESULTS AND DISCUSSION

**Constraining the ROO-H RO<sub>2</sub> H-Shift.** As shown in the Supporting Information and Figure S6, only at very high [NO] are any changes in the ratio within the 2,3 HPN observed. From data obtained at [NO] > 1 ppmv, we infer that the forward and reverse rate coefficients for the H-shifts between the 2,3 hydroperoxy RO<sub>2</sub> are about 10<sup>2</sup> s<sup>-1</sup> at 296 K and even faster (>10<sup>4</sup> s<sup>-1</sup>, 296 K) for the 2,4 hydroperoxy RO<sub>2</sub>. These are in agreement with the calculated rate coefficients of ~10<sup>3</sup> s<sup>-1</sup> and ~10<sup>6</sup> s<sup>-1</sup> for the 2,3 and 2,4 RO<sub>2</sub>, respectively. The rapid RO<sub>2</sub> isomerization of hydroperoxy hydrogens was suggested in the computational study of Jørgensen et al.,<sup>44</sup> but to the best of our knowledge, this is the first experimentally derived estimate of these rate coefficients. These rapid

isomerization reactions are critical to our study as they enable the two alkyl H-shifts (shown in Schemes 2 and 3) that are inaccessible in the initially produced RO<sub>2</sub> (see Scheme 1).

**RO<sub>2</sub> Equilibrium.** For [NO] < 100 ppb, we find that the ratios of the two HPN in the 2,3 and 2,4 RO<sub>2</sub> systems are invariant. The ratios of the HPN for the equilibrated 2,3 and 2,4 RO<sub>2</sub> systems are listed in Table 1. Because we do not know if both the branching ratio to form HPN and  $k_{\text{RO}_2+\text{NO}}$  are the same for the two isomers in each system, the ratio of the HPN signals (Table 1) may not be the same as the ratio of the concentrations of the peroxy radicals that produced them. Using the recommended branching ratio parametrization described in Wennberg et al.,<sup>85</sup> for example, the fraction of tertiary peroxy radicals is 25% smaller than estimated from the ratio of the HPNs. Table 1 also includes the equilibrium constants for the RO<sub>2</sub> calculated from the relative energies of the two RO<sub>2</sub> isomers. A 1 kcal/mol error in the difference in the free energies of the RO<sub>2</sub> (the expected accuracy of the F12 calculations) would correspond to a factor of ~5 in this ratio (at 296 K) suggesting that the calculations are consistent with the observed product distribution to within error.

**Constraining the ROO-H to Alkoxy H-Shift.** Recall from Scheme 2 that, in addition to HPN formation, alkoxy radicals are produced in the RO<sub>2</sub> + NO reaction. These alkoxy radicals undergo rapid H-shifts from the hydroperoxide to the alkoxy radicals, producing hydroxy-substituted RO<sub>2</sub> as shown in Scheme 3. Note that the reverse of this reaction (RO<sub>2</sub> abstraction of the hydroxy H) is too slow to compete over the range of lifetimes probed in our experiments.<sup>86</sup> The alkoxy H-shifts, however, are so fast that we are unable to provide a direct experimental constraint. We considered the possibility that chemical activation may play a role, but the rate coefficients derived from our calculations with the thermalized alkoxy radicals are consistent with experimental observations.

Reaction of the hydroxy-substituted RO<sub>2</sub> with NO yields the HN detected by the GC-CIMS. As shown in Figure 1C, we even observe the 2,3 HN, suggesting that these alkoxy H-shifts are at least partially competitive with  $\beta$ -scission. Using a structure-activity relationship, the energetic barrier for the 2,3 alkoxy  $\beta$ -scission is estimated to be small (<3 kcal/mol) corresponding to  $k_{\beta\text{-scission}} \sim 10^{11}$  s<sup>-1</sup>.<sup>87</sup> For the 2,3 alkoxy radicals at 296 K, the fastest alkyl H-shift is orders of magnitude slower ( $k_{\text{alkyl-H-shift}} \sim 10^5$  s<sup>-1</sup>) and thus does not compete with either  $\beta$ -scission or the rapid ROO-H 1,5 H-shift.<sup>88</sup>

For the 2,4 alkoxy radicals at 296 K,  $k_{\beta\text{-scission}}$  and  $k_{\text{alkyl-H-shift}}$  are each estimated to be <10<sup>4</sup> s<sup>-1</sup> and <10<sup>6</sup> s<sup>-1</sup>,

**Table 2. MC-TST Calculated Rate Coefficients for Selected H-shifts of Alkyl Hydrogens at 298.15 K for the Reference RO<sub>2</sub>, with the Abstracted Hydrogen Shown Explicitly in Bold**

Origin	2,3 RO <sub>2</sub>		ROO-H abstraction		
RO <sub>2</sub>					
Rate coefficient (s <sup>-1</sup> )	<b>5.3 × 10<sup>-4</sup></b>	<b>1.8 × 10<sup>-7</sup></b>	2.8 × 10 <sup>-4</sup>	5.4 × 10 <sup>-6</sup>	2.4 × 10 <sup>-4</sup>

respectively.<sup>87,88</sup> Thus, the ROO-H 1,6 H-shift rate coefficients must be similar to, or greater than,  $k_{\text{alkyl-H-shift}}$  in order to explain the observations. Consistent with this, the calculated rate coefficient for the 1,6 H-shift is  $\sim 10^{10} \text{ s}^{-1}$ . The similar ratio of HPN and HN described in Table 1 suggests that the ROO-H 1,6 H-shift is likely the only fate of the alkoxy radical.

**Determination of the 1,5  $\alpha$ -OOH H-Shift.** For both the hydroperoxy- and hydroxy-substituted RO<sub>2</sub>, we use MC-TST calculations to identify RO<sub>2</sub> isomers that do not undergo alkyl H-shifts over the range of  $\tau_{\text{bimolecular}}$  probed in the experiments (see Table 2). The total lifetime of these RO<sub>2</sub> isomers (labeled "reference" in Schemes 2 and 3) is  $\tau_{\text{bimolecular}}$  (eq 1).

The RO<sub>2</sub> that react via  $\alpha$ -OOH or  $\alpha$ -OH H-shifts ( $k_{\text{H-shift}}$ ), however, have shorter lifetimes. For these RO<sub>2</sub>, the yield of RONO<sub>2</sub> relative to that of the RONO<sub>2</sub> produced from the reference RO<sub>2</sub> will decrease as  $\tau_{\text{bimolecular}}$  is extended. The changing ratio of the RONO<sub>2</sub> isomer yields as a function of  $\tau_{\text{bimolecular}}$  is used to determine the rate coefficients of unimolecular chemistry. Enantiomeric RO<sub>2</sub> pairs are assumed to react with equal rate coefficients and are not distinguished here.

As shown in Figures 2 and 3, the ratio of both the 2,4 HPN isomers relative to the 2,3 HPN reference decreases at longer  $\tau_{\text{bimolecular}}$  as a result of the  $\alpha$ -OOH 1,5 H-shift (see Scheme 2). H-shifts arising from the 2,3 RO<sub>2</sub> are calculated to be negligible under the conditions of these experiments, and so  $\tau_{2,3 \text{ RO}_2} = \tau_{\text{bimolecular}}$  (see the first two columns in Table 2). We use the observed change in the ratio of the 2,4 HPN normalized to the 2,3 HPN as a function of  $\tau_{\text{bimolecular}}$  to infer the rate coefficient of the 1,5  $\alpha$ -OOH H-shift (Figure 3).

The rate of unimolecular chemistry inferred from the behavior shown in Figure 3,  $k_{\text{H-shift-effective}}$  is less than the rate of the isomer-specific 1,5  $\alpha$ -OOH 4-hydroperoxy-2-methyl-2-peroxy (2-OO-4-OOH) H-shift,  $k_{\text{H-shift-2-OO-4-OOH}}$ , because of the rapid interconversion between the 2,4 RO<sub>2</sub> isomers (see Scheme 2). Due to this interconversion, the concentrations of both 2,4 RO<sub>2</sub> isomers, relative to the 2,3 RO<sub>2</sub> isomers, decline at the same rate (see Figure 2). Thus, the experimentally determined rate coefficient of unimolecular chemistry is proportional to the fraction of the 2,4 RO<sub>2</sub> that is capable of the  $\alpha$ -OOH H-shift:

$$k_{\text{H-shift-effective}} = k_{\text{H-shift-2-OO-4-OOH}} \left( \frac{2\text{-OO-4-OOH}}{2\text{-OO-4-OOH} + 2\text{-OOH-4-OO}} \right)$$

For example, as the two 2,4 RO<sub>2</sub> are nearly equally abundant at equilibrium,  $k_{\text{H-shift-effective}}$  would be about half of  $k_{\text{H-shift-2-OO-4-OOH}}$ . In our experiments, the equivalence point, where the rate of unimolecular and bimolecular chemistry for the 2,4 RO<sub>2</sub> is the same, is  $\sim 0.02 \text{ s}^{-1}$ . This is  $k_{\text{H-shift-effective}}$ . This challenge of estimating isomer-specific H-shift rate coefficients in the context of an interconnected pool

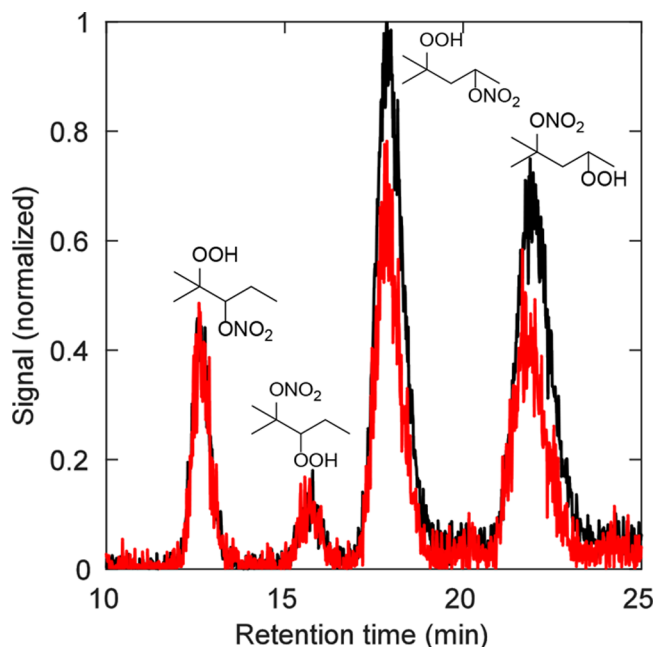


**Figure 2.** Two chromatograms following 2-hydroperoxy-2-methylpentane oxidation at 318 K are displayed. The loss of the 2,4 HPN is apparent in the experiment at  $\tau_{\text{bimolecular}} \approx 5 \text{ s}$  (red) compared to the experiment at  $\tau_{\text{bimolecular}} \approx 0.1 \text{ s}$  (black). Measurement of the ratio 2,4 HPN:2,3 HPN as a function of bimolecular lifetime is used to estimate the  $\alpha$ -OOH H-shift. The black line chromatogram has been normalized to the intensity of the tallest peak, while that of the red line has been normalized to the 2,3 HPN reference.

of RO<sub>2</sub> is similar to that described in Teng et al. for the 1,6 H-shifts in the hydroxy peroxy radicals formed following addition of OH and O<sub>2</sub> to isoprene.<sup>84</sup>

The kinetic model, shown in the curved lines in Figure 3, uses the calculated rate coefficient for the 1,5  $\alpha$ -OOH RO<sub>2</sub> H-shift (Table 3) together with an estimate of the fraction of the 2,4 RO<sub>2</sub> that exists as the 2-OO-4-OOH isomer (about 50% given the nearly equal abundance of HPN (and HN) isomers). The small difference between the HPN and HN ratios (Table 1) can be explained if the nitrate yield from the secondary RO<sub>2</sub> is 25% greater than that of the tertiary RO<sub>2</sub>. Given the uncertainties in the nitrate yields, we assume the ratio of the 2-OO-4-OOH to the 2-OOH-4-OO is no smaller than 3:1 and no larger than 1:3. Thus, we assume

$$\frac{2\text{-OO-4-OOH}}{2\text{-OO-4-OOH} + 2\text{-OOH-4-OO}} = 0.50 \pm 0.25$$

As discussed below, the measured and calculated  $k_{\text{H-shift-effective}}$  are in good agreement.

The observed temperature dependence provides further confidence in our interpretation of the mechanism responsible for the reduced yields of the 2,4 HPN isomers at long

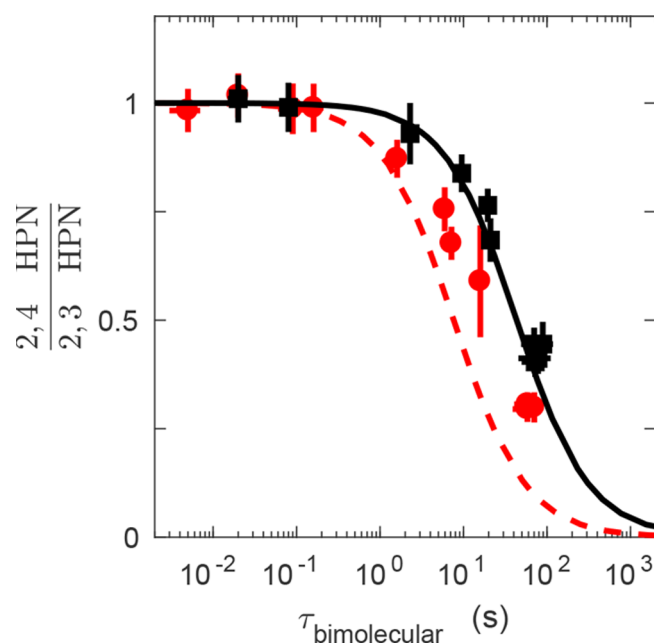


**Figure 3.** Experimental data used to constrain the 1,5  $\alpha$ -OOH H-shift at 296 K (black squares) and 318 K (red circles). The solid black (296 K) and dashed red (318 K) lines are simulations using the calculated 1,5  $\alpha$ -OOH H-shift rate together with the assumption that the concentration of the 2-OO-4-OOH isomer is equal to that of the 2-OOH-4-OO isomer. Both the model and experimental points have been normalized by the mean of the ratio obtained at the two shortest  $\tau_{\text{bimolecular}}$ . Due to the limitations of our method, it is not possible to lengthen  $\tau_{\text{bimolecular}}$  beyond 100 s; thus, the sigmoidal tail at long lifetimes is poorly constrained.

**Table 3.  $\alpha$ -OOH and  $\alpha$ -OH H-Shift Rate Coefficients ( $\text{s}^{-1}$ ) Derived by Theory and Experiment<sup>a</sup>**

Temperature	Method	Reactant		
				
		1,5 $\alpha$ -OOH H-shift	1,5 $\alpha$ -OH H-shift	1,5 $\alpha$ -OH H-shift <sup>a</sup>
296 K	Theory <sup>b</sup>	0.045	0.28	0.12
	Expt. <sup>c</sup>	$0.036^{+0.077}_{-0.027}$	$0.22^{+0.14}_{-0.040}$	$0.048^{+0.036}_{-0.024}$
318 K	Theory <sup>b</sup>	0.25	1.4	0.61
	Expt. <sup>c</sup>	$0.13^{+0.23}_{-0.10}$	$0.56^{+0.44}_{-0.14}$	$0.31^{+0.18}_{-0.061}$

<sup>a</sup>Key: (a) Reported in Praske et al.<sup>32</sup> Rate coefficients correspond to the average of the S,R and S,S diastereomers. (b) For the temperature dependent rate expressions, refer to the [Supporting Information](#). Uncertainty in the calculated rates is estimated to be less than a factor of 10.<sup>32</sup> (c) Uncertainty is estimated as described in the [Supporting Information](#). Additionally, the 1,5  $\alpha$ -OOH H-shift is sensitive to our estimate of  $K_{\text{eq}}$ . We include the uncertainty in this parameter in the reported error bounds.

$\tau_{\text{bimolecular}}$ . The equivalence point, where  $k_{\text{RO}_2+\text{NO}}[\text{NO}] + k_{\text{RO}_2+\text{HO}_2}[\text{HO}_2] = k_{\text{H-shift-effective}}$  occurs when  $\tau_{\text{bimolecular}}$  is  $\sim 4$  times shorter at 318 K than at 296 K, consistent with the large energetic barriers encountered by these H-shifts (see [Supporting Information](#)).

**Determination of the 1,5  $\alpha$ -OH  $k_{\text{H-shift}}$ .** The 1,5  $\alpha$ -OH H-shift of the 4-hydroxy-2-methyl-2-peroxy isomer is observed using measurements of the HN ([Scheme 3](#)), and the rate

coefficient is quantified in a manner similar to that used in the determination of the 1,5  $\alpha$ -OOH H-shift. In this system, the 2-hydroxy-2-methyl-5-nitrooxy isomer is used as a reference. Our calculations ([Table 2](#)) demonstrate negligible H-shift channels for the  $\text{RO}_2$  formed via the  $\text{ROO-H}$  abstraction of 2-hydroperoxy-2-methylpentane (left column in [Scheme 3](#)). This  $\text{RO}_2$  reacts with NO and the resulting alkoxy undergoes a 1,5 H-shift to produce a hydroxy-substituted  $\text{RO}_2$ , which also exhibits a negligible H-shift pathway ([Table 2](#)). Thus, the HN arising from reaction of this  $\text{RO}_2$  with NO serves as a suitable reference.

As shown in [Figure 4](#), the ratio of the yield of the 4-hydroxy-2-methyl-2-nitrooxy isomer to that of the 2-hydroxy-2-methyl-

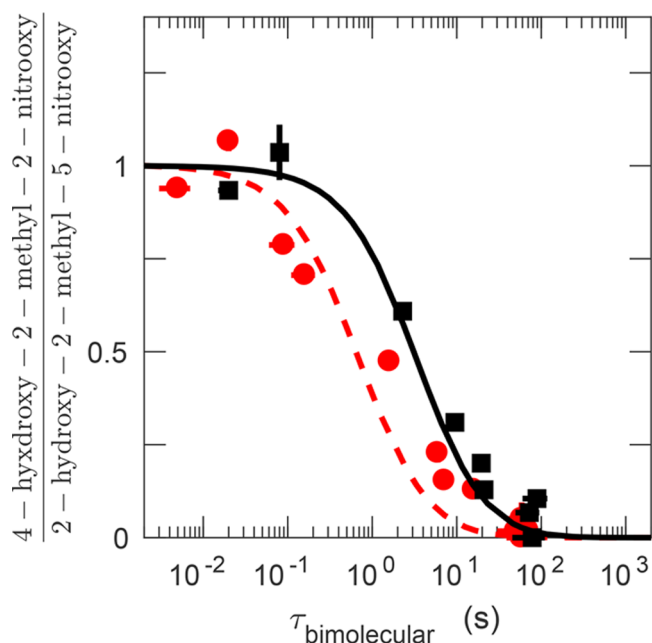


**Figure 4.** Experimental data used to constrain the 1,5  $\alpha$ -OH H-shift at 296 K (black squares) and 318 K (red circles). Simulated curves using computational results for the  $\alpha$ -OH H-shift are shown at 296 K (solid black) and 318 K (dashed red). The simulations use the experimentally constrained rate coefficient for the 1,5  $\alpha$ -OOH H-shift ([Table 3](#)), while the calculated rate coefficient is used for the 1,5  $\alpha$ -OH H-shift. Both the model and experimental points have been normalized by the mean of the ratio obtained at the two shortest  $\tau_{\text{bimolecular}}$ .

5-nitrooxy reference exhibits a strong dependence on  $\tau_{\text{bimolecular}}$  and temperature. The process responsible for this dependence is assigned to a 1,5 H-shift proceeding via abstraction of the  $\alpha$ -OH hydrogen ([Scheme 3](#)). In [Figure 4](#), the kinetic model employs the theoretically calculated  $\alpha$ -OH H-shift rate coefficient. However, the curve shown in [Figure 4](#) also depends on both the rapid hydrogen scrambling between the  $\text{RO}_2$  isomers as well as the  $\alpha$ -OOH H-shift rate coefficient since the production of the 2,4 HN is tied to the 2,4  $\text{RO}_2$  system ([Scheme 3](#)). Here, we use the experimentally constrained 1,5  $\alpha$ -OOH H-shift rate coefficient, and the error bounds in [Table 3](#) account for the full range of uncertainty in this value.

**Products of the 1,5 H-Shift Chemistry.** A significant CIMS signal is observed at  $m/z$  217, corresponding to the cluster of a compound of nominal mass 132 amu and the  $\text{CF}_3\text{O}^-$  reagent ion,  $m/z$  85. As in our previous study, this

signal is attributed to the formation of the ketohydroperoxide,<sup>32</sup> a product of the autoxidation mechanism following hydrogen abstraction at  $\alpha$ -OH and  $\alpha$ -OOH centers as shown in Schemes 2 and 3. There is only one ketohydroperoxide isomer produced by both of these H-shifts.

**Comparison of Experimental and Computational Results.** The experimental rate coefficients shown in Table 3 are derived by fitting the kinetic model to the experimental data (see Supporting Information, Figures S4 and S5). The experimental and calculated values agree to better than a factor of 3. Furthermore, reasonable agreement is achieved by comparison of our results with those of Mohamed et al.<sup>38</sup> Although the study focused on temperature ranges relevant to combustion, the 1,5  $\alpha$ -OOH H-shift rate coefficient was calculated to be  $0.07 \text{ s}^{-1}$  at 296 K and  $0.5 \text{ s}^{-1}$  at 318 K, within a factor of 4 of our experimental and computational results (see Table 3). In combination with our previous results,<sup>32</sup> the reasonable agreement suggests that the computational approach used here, and described in detail by Møller et al.,<sup>51</sup> is a robust method for calculating the kinetic parameters of RO<sub>2</sub> H-shifts for the diverse substrates needed to be considered in chemical models.

**Role of Structure.** At 296 K, the experimentally determined rate coefficient of the  $\alpha$ -OH 1,5 H-shift is  $\sim 5$  times greater than that of the  $\alpha$ -OH 1,5 H-shift in a peroxy radical produced in the oxidation of 2-hexanol (see Table 3).<sup>32</sup> The difference in these rate coefficients for nominally similar H-shifts clearly demonstrates that structure plays a key role in the kinetics.

The effect of structure has previously been investigated computationally in unimolecular reactions involved in fuel combustion at elevated temperatures. Miyoshi, for example, determined that increasing the methyl substitution of the RO<sub>2</sub> center increases the reaction barrier in 1,7 H-shifts.<sup>37</sup> This effect was attributed to an increase in the ring strain energy of the transition state, likely caused by the spatial configuration of the methyl substituents. Similarly, Davis and Francisco computationally investigated H-shifts in *n*-alkyl and branched methyl alkyl radicals,<sup>89,90</sup> and found that the spatial configuration of the methyl substituent influenced the energy of the transition state. This effect was correlated to a shift of the methyl group from a gauche to anti configuration, which produced lower barrier heights. Otkjær et al. computationally studied a systematic set of peroxy radicals with a range of different substituents.<sup>33</sup> They calculated that the presence of an  $\alpha$ -OH or  $\alpha$ -OOH group can increase the rate coefficient of an H-shift by factors up to 1000, in agreement with the experimental results of our current and previous work.<sup>32</sup> Finally, hydrogen bond-like interactions in the reactant and transition state influence the barrier height, as previously demonstrated.<sup>32,86</sup>

**Atmospheric Implications.** In this study, we demonstrate the migration of hydroperoxy hydrogens in alkoxy and peroxy radicals. The rate coefficients are sufficiently large that this chemistry will outrun bimolecular reaction in the atmosphere for similar radicals. Additionally, these processes are competitive even under typical “high NO” conditions employed in chamber studies, suggesting a possible role for these reactions in explaining the shortcomings of previous mechanistic interpretations. Perhaps of equal importance is the ability of alkoxy radicals to abstract hydroperoxy hydrogens fast enough to compete against fast unimolecular processes including  $\beta$ -scission and alkyl isomerization.

The rapid scrambling of the radical center enables subsequent autoxidation pathways that are otherwise inaccessible. For example, the  $\alpha$ -OH and  $\alpha$ -OOH H-shifts quantified in this work are not accessible without this chemistry due to the presence of the  $\alpha$ -methyl substituent in the precursor. This suggests that reaction mechanisms must account for the migration of hydroperoxy hydrogens in order to capture the atmospheric fate of these species. Due to ongoing NO<sub>x</sub> emission reductions,<sup>91</sup> such organic hydroperoxides formed through both HO<sub>2</sub> chemistry and autoxidation will comprise an increasingly large share of reactive atmospheric trace gases.

This study emphasizes the need to understand the fate of these autoxidation products. In alkane oxidation, we have shown that ketohydroperoxides are significant products. In order to better assess their role in the urban atmosphere as it relates to air quality, a study that quantitatively examines the fate of ketohydroperoxides (e.g., photolysis, deposition, oxidation, or aerosol transfer) is needed.

## ■ ASSOCIATED CONTENT

### 📄 Supporting Information

The Supporting Information is available free of charge on the ACS Publications website at DOI: 10.1021/acs.jpca.8b09745.

Synthesis, calibration factors, NMR spectra, chromatographic analysis, uncertainty, additional computational results, and temperature-dependent rate expressions (PDF)

## ■ AUTHOR INFORMATION

### Corresponding Authors

\*(P.O.W.) E-mail: [wennberg@caltech.edu](mailto:wennberg@caltech.edu).

\*(H.G.K.) E-mail: [hgk@chem.ku.dk](mailto:hgk@chem.ku.dk).

### ORCID

Rasmus V. Otkjær: 0000-0002-6094-1828

John D. Crouse: 0000-0001-5443-729X

Brian M. Stoltz: 0000-0001-9837-1528

Henrik G. Kjaergaard: 0000-0002-7275-8297

Paul O. Wennberg: 0000-0002-6126-3854

### Notes

The authors declare no competing financial interest.

The wB97X-D/aug-cc-pVTZ optimizations and frequencies and the CCSD(T)-F12a/VDZ-F12 single point energy calculations are available at <https://sid.erda.dk/public/archives/4f4b98346d6b007ba44411c642b39fa1/published-archive.html>.

## ■ ACKNOWLEDGMENTS

J.C.H. thanks the Camille and Henry Dreyfus postdoctoral program in Environmental Chemistry for support. We acknowledge funding from the National Science Foundation (Grant CHE-1508526), the University of Copenhagen, and the Danish Center for Scientific Computing.

## ■ REFERENCES

- (1) Seinfeld, J. H.; Pandis, S. N. *Atmospheric Chemistry and Physics: From Air Pollution to Climate Change*. Wiley: New York, 1998.
- (2) Orlando, J. J.; Tyndall, G. S. *Laboratory Studies of Organic Peroxy Radical Chemistry: An Overview with Emphasis on Recent Issues of Atmospheric Significance*. *Chem. Soc. Rev.* **2012**, *41* (19), 6294–6317.

- (3) Peeters, J.; Nguyen, T. L.; Vereecken, L. HO<sub>x</sub> Radical Regeneration in the Oxidation of Isoprene. *Phys. Chem. Chem. Phys.* **2009**, *11* (28), 5935–5939.
- (4) Asatryan, R.; da Silva, G.; Bozzelli, J. W. Quantum Chemical Study of the Acrolein (CH<sub>2</sub>CHCHO) + OH + O<sub>2</sub> Reactions. *J. Phys. Chem. A* **2010**, *114* (32), 8302–8311.
- (5) Crouse, J. D.; Paulot, F.; Kjaergaard, H. G.; Wennberg, P. O. Peroxy Radical Isomerization in the Oxidation of Isoprene. *Phys. Chem. Chem. Phys.* **2011**, *13* (30), 13607–13613.
- (6) Vereecken, L.; Francisco, J. S. Theoretical Studies of Atmospheric Reaction Mechanisms in the Troposphere. *Chem. Soc. Rev.* **2012**, *41* (19), 6259–6293.
- (7) Crouse, J. D.; Knap, H. C.; Ørnso, K. B.; Jørgensen, S.; Paulot, F.; Kjaergaard, H. G.; Wennberg, P. O. Atmospheric Fate of Methacrolein. 1. Peroxy Radical Isomerization Following Addition of OH and O<sub>2</sub>. *J. Phys. Chem. A* **2012**, *116* (24), 5756–5762.
- (8) Crouse, J. D.; Nielsen, L. B.; Jørgensen, S.; Kjaergaard, H. G.; Wennberg, P. O. Autoxidation of Organic Compounds in the Atmosphere. *J. Phys. Chem. Lett.* **2013**, *4* (20), 3513–3520.
- (9) Knap, H. C.; Jørgensen, S.; Kjaergaard, H. G. Theoretical Investigation of the Hydrogen Shift Reactions in Peroxy Radicals Derived from the Atmospheric Decomposition of 3-methyl-3-buten-1-ol (MBO331). *Chem. Phys. Lett.* **2015**, *619*, 236–240.
- (10) Jokinen, T.; Sipilä, M.; Richters, S.; Kerminen, V.; Paasonen, P.; Stratmann, F.; Worsnop, D.; Kulmala, M.; Ehn, M.; Herrmann, H.; et al. Rapid Autoxidation Forms Highly Oxidized RO<sub>2</sub> Radicals in the Atmosphere. *Angew. Chem., Int. Ed.* **2014**, *53* (52), 14596–14600.
- (11) Kurtén, T.; Rissanen, M. P.; Mackeprang, K.; Thornton, J. A.; Hyttinen, N.; Jørgensen, S.; Ehn, M.; Kjaergaard, H. G. Computational Study of Hydrogen Shifts and Ring-Opening Mechanisms in  $\alpha$ -Pinene Ozonolysis Products. *J. Phys. Chem. A* **2015**, *119* (46), 11366–11375.
- (12) Richters, S.; Herrmann, H.; Berndt, T. Highly Oxidized RO<sub>2</sub> Radicals and Consecutive Products from the Ozonolysis of Three Sesquiterpenes. *Environ. Sci. Technol.* **2016**, *50* (5), 2354–2362.
- (13) Wang, S.; Wu, R.; Berndt, T.; Ehn, M.; Wang, L. Formation of Highly Oxidized Radicals and Multifunctional Products from the Atmospheric Oxidation of Alkylbenzenes. *Environ. Sci. Technol.* **2017**, *51* (15), 8442–8449.
- (14) Xu, L.; Møller, K. H.; Crouse, J. D.; Otkjær, R. V.; Kjaergaard, H. G.; Wennberg, P. O. Unimolecular Reactions of Peroxy Radicals Formed in the Oxidation of  $\alpha$ -Pinene and  $\beta$ -Pinene by Hydroxyl Radicals, Manuscript under review for *J. Phys. Chem. A*.
- (15) Savee, J. D.; Papajak, E.; Rotavera, B.; Huang, H.; Eskola, A. J.; Welz, O.; Sheps, L.; Taatjes, C. A.; Zádor, J.; Osborn, D. L. Direct Observation and Kinetics of a Hydroperoxyalkyl Radical (QOOH). *Science* **2015**, *347* (6222), 643–646.
- (16) Taatjes, C. A. Uncovering the Fundamental Chemistry of Alkyl + O<sub>2</sub> Reactions Via Measurements of Product Formation. *J. Phys. Chem. A* **2006**, *110* (13), 4299–4312.
- (17) Zádor, J.; Taatjes, C. A.; Fernandes, R. X. Kinetics of Elementary Reactions in Low-Temperature Autoignition Chemistry. *Prog. Energy Combust. Sci.* **2011**, *37* (4), 371–421.
- (18) Ehn, M.; Thornton, J. A.; Kleist, E.; Sipilä, M.; Junninen, H.; Pullinen, I.; Springer, M.; Rubach, F.; Tillmann, R.; Lee, B.; et al. A Large Source of Low-Volatility Secondary Organic Aerosol. *Nature* **2014**, *506* (7489), 476–479.
- (19) Zhang, X.; Lambe, A. T.; Upshur, M. A.; Brooks, W. A.; Gray Bé, A.; Thomson, R. J.; Geiger, F. M.; Surratt, J. D.; Zhang, Z.; Gold, A.; et al. Highly Oxygenated Multifunctional Compounds in  $\alpha$ -Pinene Secondary Organic Aerosol. *Environ. Sci. Technol.* **2017**, *51* (11), 5932–5940.
- (20) Berndt, T.; Richters, S.; Jokinen, T.; Hyttinen, N.; Kurtén, T.; Otkjær, R. V.; Kjaergaard, H. G.; Stratmann, F.; Herrmann, H.; Sipilä, M.; et al. Hydroxyl Radical-Induced Formation of Highly Oxidized Organic Compounds. *Nat. Commun.* **2016**, *7*, 13677.
- (21) Jokinen, T.; Berndt, T.; Makkonen, R.; Kerminen, V.-M.; Junninen, H.; Paasonen, P.; Stratmann, F.; Herrmann, H.; Guenther, A. B.; Worsnop, D. R.; et al. Production of Extremely Low Volatile Organic Compounds from Biogenic Emissions: Measured Yields and Atmospheric Implications. *Proc. Natl. Acad. Sci. U. S. A.* **2015**, *112* (23), 7123–7128.
- (22) Mentel, T. F.; Springer, M.; Ehn, M.; Kleist, E.; Pullinen, I.; Kurtén, T.; Rissanen, M.; Wahner, A.; Wildt, J. Formation of Highly Oxidized Multifunctional Compounds: Autoxidation of Peroxy Radicals Formed in the Ozonolysis of Alkenes – Deduced from Structure–Product Relationships. *Atmos. Chem. Phys.* **2015**, *15* (12), 6745–6765.
- (23) Zhang, X.; McVay, R. C.; Huang, D. D.; Dalleska, N. F.; Aumont, B.; Flagan, R. C.; Seinfeld, J. H. Formation and Evolution of Molecular Products in  $\alpha$ -Pinene Secondary Organic Aerosol. *Proc. Natl. Acad. Sci. U. S. A.* **2015**, *112* (46), 14168–14173.
- (24) Mutzel, A.; Poulain, L.; Berndt, T.; Iinuma, Y.; Rodigast, M.; Böge, O.; Richters, S.; Spindler, G.; Sipilä, M.; Jokinen, T.; et al. Highly Oxidized Multifunctional Organic Compounds Observed in Tropospheric Particles: A Field and Laboratory Study. *Environ. Sci. Technol.* **2015**, *49* (13), 7754–7761.
- (25) Kirkby, J.; Duplissy, J.; Sengupta, K.; Frege, C.; Gordon, H.; Williamson, C.; Heinritzi, M.; Simon, M.; Yan, C.; Almeida, J.; et al. Ion-Induced Nucleation of Pure Biogenic Particles. *Nature* **2016**, *533* (7604), 521–526.
- (26) Schobesberger, S.; Junninen, H.; Bianchi, F.; Lönn, G.; Ehn, M.; Lehtipalo, K.; Dommen, J.; Ehrhart, S.; Ortega, I. K.; Franchin, A.; et al. Molecular Understanding of Atmospheric Particle Formation from Sulfuric Acid and Large Oxidized Organic Molecules. *Proc. Natl. Acad. Sci. U. S. A.* **2013**, *110* (43), 17223–17228.
- (27) Riccobono, F.; Schobesberger, S.; Scott, C. E.; Dommen, J.; Ortega, I. K.; Rondo, L.; Almeida, J.; Amorim, A.; Bianchi, F.; Breitenlechner, M.; et al. Oxidation Products of Biogenic Emissions Contribute to Nucleation of Atmospheric Particles. *Science* **2014**, *344* (6185), 717–721.
- (28) Zhao, J.; Ortega, J.; Chen, M.; McMurry, P. H.; Smith, J. N. Dependence of Particle Nucleation and Growth on High-Molecular-Weight Gas-Phase Products During Ozonolysis of  $\alpha$ -Pinene. *Atmos. Chem. Phys.* **2013**, *13* (15), 7631–7644.
- (29) Bianchi, F.; Tröstl, J.; Junninen, H.; Frege, C.; Henne, S.; Hoyle, C. R.; Molteni, U.; Herrmann, E.; Adamov, A.; Bukowiecki, N.; et al. New Particle Formation in the Free Troposphere: A Question of Chemistry and Timing. *Science* **2016**, *352* (6289), 1109–12.
- (30) Kulmala, M.; Kontkanen, J.; Junninen, H.; Lehtipalo, K.; Manninen, H. E.; Nieminen, T.; Petäjä, T.; Sipilä, M.; Schobesberger, S.; Rantala, P.; et al. Direct Observations of Atmospheric Aerosol Nucleation. *Science* **2013**, *339* (6122), 943–946.
- (31) Stolzenburg, D.; Fischer, L.; Vogel, A. L.; Heinritzi, M.; Schervish, M.; Simon, M.; Wagner, A. C.; Dada, L.; Ahonen, L. R.; Amorim, A.; et al. Rapid Growth of Organic Aerosol Nanoparticles over a Wide Tropospheric Temperature Range. *Proc. Natl. Acad. Sci. U. S. A.* **2018**, *115* (37), 9122–9127.
- (32) Praske, E.; Otkjær, R. V.; Crouse, J. D.; Hethcox, J. C.; Stoltz, B. M.; Kjaergaard, H. G.; Wennberg, P. O. Atmospheric Autoxidation Is Increasingly Important in Urban and Suburban North America. *Proc. Natl. Acad. Sci. U. S. A.* **2018**, *115* (1), 64–69.
- (33) Otkjær, R. V.; Jakobsen, H. H.; Tram, C. M.; Kjaergaard, H. G. Calculated Hydrogen Shift Rate Constants in Substituted Alkyl Peroxy Radicals. *J. Phys. Chem. A* **2018**, *122* (43), 8665–8673.
- (34) Jorand, F.; Heiss, A.; Perrin, O.; Sahetchian, K.; Kerhoas, L.; Einhorn, J. Isomeric Hexyl-Ketohydroperoxides Formed by Reactions of Hexoxy and Hexylperoxy Radicals in Oxygen. *Int. J. Chem. Kinet.* **2003**, *35* (8), 354–366.
- (35) Liu, Z.; Nguyen, V. S.; Harvey, J.; Muller, J.-F.; Peeters, J. The Photolysis of  $\alpha$ -Hydroperoxycarbonyls. *Phys. Chem. Chem. Phys.* **2018**, *20* (10), 6970–6979.
- (36) Goldsmith, C. F.; Green, W. H.; Klippenstein, S. J. Role of O<sub>2</sub> + QOOH in Low-Temperature Ignition of Propane. 1. Temperature and Pressure Dependent Rate Coefficients. *J. Phys. Chem. A* **2012**, *116* (13), 3325–3346.

- (37) Miyoshi, A. Systematic Computational Study on the Unimolecular Reactions of Alkylperoxy (RO<sub>2</sub>), Hydroperoxyalkyl (QOOH), and Hydroperoxyalkylperoxy (O<sub>2</sub>QOOH) Radicals. *J. Phys. Chem. A* **2011**, *115* (15), 3301–3325.
- (38) Mohamed, S. Y.; Davis, A. C.; Al Rashidi, M. J.; Sarathy, S. M. High-Pressure Limit Rate Rules for  $\alpha$ -H Isomerization of Hydroperoxyalkylperoxy Radicals. *J. Phys. Chem. A* **2018**, *122* (14), 3626–3639.
- (39) Sharma, S.; Raman, S.; Green, W. H. Intramolecular Hydrogen Migration in Alkylperoxy and Hydroperoxyalkylperoxy Radicals: Accurate Treatment of Hindered Rotors. *J. Phys. Chem. A* **2010**, *114* (18), 5689–5701.
- (40) Yao, Q.; Sun, X.-H.; Li, Z.-R.; Chen, F.-F.; Li, X.-Y. Pressure-Dependent Rate Rules for Intramolecular H-Migration Reactions of Hydroperoxyalkylperoxy Radicals in Low Temperature. *J. Phys. Chem. A* **2017**, *121* (16), 3001–3018.
- (41) Asatryan, R.; Bozzelli, J. W. Chain Branching and Termination in the Low-Temperature Combustion of n-Alkanes: 2-Pentyl Radical + O<sub>2</sub>, Isomerization and Association of the Second O<sub>2</sub>. *J. Phys. Chem. A* **2010**, *114* (29), 7693–7708.
- (42) Wang, Z.; Popolan-Vaida, D. M.; Chen, B.; Moshhammer, K.; Mohamed, S. Y.; Wang, H.; Sioud, S.; Raji, M. A.; Kohse-Höinghaus, K.; Hansen, N.; et al. Unraveling the Structure and Chemical Mechanisms of Highly Oxygenated Intermediates in Oxidation of Organic Compounds. *Proc. Natl. Acad. Sci. U. S. A.* **2017**, *114* (50), 13102–13107.
- (43) Sha, Y.; Dibble, T. S. Tunneling Effect in 1,5 H-Migration of a Prototypical OOQOOH. *Chem. Phys. Lett.* **2016**, *646*, 153–157.
- (44) Jørgensen, S.; Knap, H. C.; Otkjær, R. V.; Jensen, A. M.; Kjeldsen, M. L. H.; Wennberg, P. O.; Kjaergaard, H. G. Rapid Hydrogen Shift Scrambling in Hydroperoxy-Substituted Organic Peroxy Radicals. *J. Phys. Chem. A* **2016**, *120* (2), 266–275.
- (45) Knap, H. C.; Jørgensen, S. Rapid Hydrogen Shift Reactions in Acyl Peroxy Radicals. *J. Phys. Chem. A* **2017**, *121* (7), 1470–1479.
- (46) Dibble, T. S. Intramolecular Hydrogen Bonding and Double H-Atom Transfer in Peroxy and Alkoxy Radicals from Isoprene. *J. Phys. Chem. A* **2004**, *108* (12), 2199–2207.
- (47) Dibble, T. S. Prompt Chemistry of Alkenoxy Radical Products of the Double H-Atom Transfer of Alkoxy Radicals from Isoprene. *J. Phys. Chem. A* **2004**, *108* (12), 2208–2215.
- (48) Eyring, H. The Activated Complex and the Absolute Rate of Chemical Reactions. *Chem. Rev.* **1935**, *17* (1), 65–77.
- (49) Evans, M. G.; Polanyi, M. Some Applications of the Transition State Method to the Calculation of Reaction Velocities, Especially in Solution. *Trans. Faraday Soc.* **1935**, *31* (0), 875–894.
- (50) Vereecken, L.; Peeters, J. The 1,5-H-Shift in 1-Butoxy: A Case Study in the Rigorous Implementation of Transition State Theory for a Multitrotamer System. *J. Chem. Phys.* **2003**, *119* (10), 5159–5170.
- (51) Møller, K. H.; Otkjær, R. V.; Hyttinen, N.; Kurtén, T.; Kjaergaard, H. G. Cost-Effective Implementation of Multiconformer Transition State Theory for Peroxy Radical Hydrogen Shift Reactions. *J. Phys. Chem. A* **2016**, *120* (51), 10072–10087.
- (52) Eckart, C. The Penetration of a Potential Barrier by Electrons. *Phys. Rev.* **1930**, *35* (11), 1303–1309.
- (53) Halgren, T. A. Merck Molecular Force Field. I. Basis, Form, Scope, Parameterization, and Performance of MMFF94. *J. Comput. Chem.* **1996**, *17* (5–6), 490–519.
- (54) Halgren, T. A. Merck Molecular Force Field. II. MMFF94 Van Der Waals and Electrostatic Parameters for Intermolecular Interactions. *J. Comput. Chem.* **1996**, *17* (5–6), 520–552.
- (55) Halgren, T. A. Merck Molecular Force Field. III. Molecular Geometries and Vibrational Frequencies for MMFF94. *J. Comput. Chem.* **1996**, *17* (5–6), 553–586.
- (56) Halgren, T. A.; Nachbar, R. B. Merck Molecular Force Field. IV. Conformational Energies and Geometries for MMFF94. *J. Comput. Chem.* **1996**, *17* (5–6), 587–615.
- (57) Halgren, T. A. Merck Molecular Force Field. V. Extension of MMFF94 Using Experimental Data, Additional Computational Data, and Empirical Rules. *J. Comput. Chem.* **1996**, *17* (5–6), 616–641.
- (58) Halgren, T. A. MMFF VII. Characterization of MMFF94, MMFF94s, and Other Widely Available Force Fields for Conformational Energies and for Intermolecular-Interaction Energies and Geometries. *J. Comput. Chem.* **1999**, *20* (7), 730–748.
- (59) *Spartan'14*; Wavefunction Inc.: Irvine, CA, 2014.
- (60) Becke, A. D. Density-Functional Thermochemistry. III. The Role of Exact Exchange. *J. Chem. Phys.* **1993**, *98* (7), 5648–5652.
- (61) Lee, C.; Yang, W.; Parr, R. G. Development of the Colle-Salvetti Correlation-Energy Formula into a Functional of the Electron Density. *Phys. Rev. B: Condens. Matter Mater. Phys.* **1988**, *37* (2), 785–789.
- (62) Hehre, W. J.; Ditchfield, R.; Pople, J. A. Self-Consistent Molecular Orbital Methods. XII. Further Extensions of Gaussian-Type Basis Sets for Use in Molecular Orbital Studies of Organic Molecules. *J. Chem. Phys.* **1972**, *56* (5), 2257–2261.
- (63) Clark, T.; Chandrasekhar, J.; Spitznagel, G. W.; Schleyer, P. V. R. Efficient Diffuse Function-Augmented Basis Sets for Anion Calculations. III. The 3-21+G Basis Set for First-Row Elements, Li–F. *J. Comput. Chem.* **1983**, *4* (3), 294–301.
- (64) Frisch, M. J.; Pople, J. A.; Binkley, J. S. Self-Consistent Molecular Orbital Methods 25. Supplementary Functions for Gaussian Basis Sets. *J. Chem. Phys.* **1984**, *80* (7), 3265–3269.
- (65) Frisch, M. J.; Trucks, G. W.; Schlegel, H. B.; Scuseria, G. E.; Robb, M. A.; Cheeseman, J. R.; Scalmani, G.; Barone, V.; Petersson, G. A.; Nakatsuji, H., et al. *Gaussian 09*, Revision D.01; Gaussian: Wallingford, CT, 2009.
- (66) Otkjær, R. V.; Møller, K. H. *Github: Removal of Duplicate Conformers V1.0*; <https://github.com/TheKjaergaardGroup/Removal-of-Duplicate-Conformers>, (accessed August 23, 2018).
- (67) Kendall, R. A.; Dunning, T. H., Jr.; Harrison, R. J. Electron Affinities of the First-Row Atoms Revisited. Systematic Basis Sets and Wave Functions. *J. Chem. Phys.* **1992**, *96* (9), 6796–6806.
- (68) Chai, J.-D.; Head-Gordon, M. Long-Range Corrected Hybrid Density Functionals with Damped Atom-Atom Dispersion Corrections. *Phys. Chem. Phys.* **2008**, *10* (44), 6615–6620.
- (69) Peterson, K. A.; Adler, T. B.; Werner, H.-J. Systematically Convergent Basis Sets for Explicitly Correlated Wavefunctions: The Atoms H, He, B–Ne, and Al–Ar. *J. Chem. Phys.* **2008**, *128* (8), 084102.
- (70) Werner, H.-J.; Knizia, G.; Manby, F. R. Explicitly Correlated Coupled Cluster Methods with Pair-Specific Geminals. *Mol. Phys.* **2011**, *109* (3), 407–417.
- (71) Adler, T. B.; Knizia, G.; Werner, H.-J. A Simple and Efficient CCSD(T)-F12 Approximation. *J. Chem. Phys.* **2007**, *127* (22), 221106.
- (72) Knizia, G.; Adler, T. B.; Werner, H.-J. Simplified CCSD(T)-F12 Methods: Theory and Benchmarks. *J. Chem. Phys.* **2009**, *130* (5), 054104.
- (73) Watts, J. D.; Gauss, J.; Bartlett, R. J. Coupled-Cluster Methods with Noniterative Triple Excitations for Restricted Open-Shell Hartree-Fock and Other General Single Determinant Reference Functions. Energies and Analytical Gradients. *J. Chem. Phys.* **1993**, *98* (11), 8718–8733.
- (74) Werner, H. J.; Knowles, P. J.; Knizia, G.; Manby, F. R.; Schutz, M. *MOLPRO, Version 2012.1, a Package of Ab Initio Programs*; 2012.
- (75) Taylor, W. D.; Allston, T. D.; Moscato, M. J.; Fazekas, G. B.; Kozłowski, R.; Takacs, G. A. Atmospheric Photo-Dissociation Lifetimes for Nitromethane, Methyl Nitrite, and Methyl Nitrate. *Int. J. Chem. Kinet.* **1980**, *12* (4), 231–240.
- (76) Sharpe, S. W.; Johnson, T. J.; Sams, R. L.; Chu, P. M.; Rhoderick, G. C.; Johnson, P. A. Gas-Phase Databases for Quantitative Infrared Spectroscopy. *Appl. Spectrosc.* **2004**, *58* (12), 1452–1461.
- (77) Vasquez, K. T.; Allen, H. M.; Crouse, J. D.; Praske, E.; Xu, L.; Noelscher, A. C.; Wennberg, P. O. Low-pressure gas chromatography with chemical ionization mass spectrometry for quantification of multifunctional organic compounds in the atmosphere. *Atmos. Meas. Tech.* **2018**, *11*, 6815–6832.

(78) Crouse, J. D.; McKinney, K. A.; Kwan, A. J.; Wennberg, P. O. Measurement of Gas-Phase Hydroperoxides by Chemical Ionization Mass Spectrometry. *Anal. Chem.* **2006**, *78* (19), 6726–6732.

(79) Paulot, F.; Crouse, J. D.; Kjaergaard, H. G.; Kroll, J. H.; Seinfeld, J. H.; Wennberg, P. O. Isoprene Photooxidation: New Insights into the Production of Acids and Organic Nitrates. *Atmos. Chem. Phys.* **2009**, *9* (4), 1479–1501.

(80) Praske, E.; Crouse, J. D.; Bates, K. H.; Kurtén, T.; Kjaergaard, H. G.; Wennberg, P. O. Atmospheric Fate of Methyl Vinyl Ketone: Peroxy Radical Reactions with NO and HO<sub>2</sub>. *J. Phys. Chem. A* **2015**, *119* (19), 4562–4572.

(81) Bates, K. H.; Crouse, J. D.; St. Clair, J. M.; Bennett, N. B.; Nguyen, T. B.; Seinfeld, J. H.; Stoltz, B. M.; Wennberg, P. O. Gas Phase Production and Loss of Isoprene Epoxydiols. *J. Phys. Chem. A* **2014**, *118* (7), 1237–1246.

(82) St. Clair, J. M.; Rivera-Rios, J. C.; Crouse, J. D.; Knap, H. C.; Bates, K. H.; Teng, A. P.; Jørgensen, S.; Kjaergaard, H. G.; Keutsch, F. N.; Wennberg, P. O. Kinetics and Products of the Reaction of the First-Generation Isoprene Hydroxy Hydroperoxide (ISOPOOH) with OH. *J. Phys. Chem. A* **2016**, *120* (9), 1441–1451.

(83) Schwantes, R. H.; Teng, A. P.; Nguyen, T. B.; Coggon, M. M.; Crouse, J. D.; St. Clair, J. M.; Zhang, X.; Schilling, K. A.; Seinfeld, J. H.; Wennberg, P. O. Isoprene NO<sub>3</sub> Oxidation Products from the RO<sub>2</sub> + HO<sub>2</sub> Pathway. *J. Phys. Chem. A* **2015**, *119* (40), 10158–10171.

(84) Teng, A. P.; Crouse, J. D.; Wennberg, P. O. Isoprene Peroxy Radical Dynamics. *J. Am. Chem. Soc.* **2017**, *139* (15), 5367–5377.

(85) Wennberg, P. O.; Bates, K. H.; Crouse, J. D.; Dodson, L. G.; McVay, R. C.; Mertens, L. A.; Nguyen, T. B.; Praske, E.; Schwantes, R. H.; Smarte, M. D.; et al. Gas-Phase Reactions of Isoprene and its Major Oxidation Products. *Chem. Rev.* **2018**, *118* (7), 3337–3390.

(86) Peeters, J.; Müller, J.-F.; Stavrakou, T.; Nguyen, V. S. Hydroxyl Radical Recycling in Isoprene Oxidation Driven by Hydrogen Bonding and Hydrogen Tunneling: The Upgraded LIM1 Mechanism. *J. Phys. Chem. A* **2014**, *118* (38), 8625–8643.

(87) Vereecken, L.; Peeters, J. Decomposition of Substituted Alkoxy Radicals-Part I: A Generalized Structure-Activity Relationship for Reaction Barrier Heights. *Phys. Chem. Chem. Phys.* **2009**, *11* (40), 9062–9074.

(88) Atkinson, R. Rate Constants for the Atmospheric Reactions of Alkoxy Radicals: An Updated Estimation Method. *Atmos. Environ.* **2007**, *41* (38), 8468–8485.

(89) Davis, A. C.; Francisco, J. S. Ab Initio Study of Hydrogen Migration across n-Alkyl Radicals. *J. Phys. Chem. A* **2011**, *115* (14), 2966–2977.

(90) Davis, A. C.; Francisco, J. S. Ab Initio Study of Key Branching Reactions in Biodiesel and Fischer–Tropsch Fuels. *J. Am. Chem. Soc.* **2011**, *133* (47), 19110–19124.

(91) Russell, A. R.; Valin, L. C.; Cohen, R. C. Trends in OMI NO<sub>2</sub> Observations over the United States: Effects of Emission Control Technology and the Economic Recession. *Atmos. Chem. Phys.* **2012**, *12* (24), 12197–12209.